ACS OMEGA

Open Access

http://pubs.acs.org/journal/acsodf

Article

Impact of Cobalt Doping on the Structural, Optical, and Dielectric Properties of $MgAl_2O_4$ Spinel Material

Kamran Ullah, Shoaib Ali Khan, Abid Zaman,* Mahidur R. Sarker, Asad Ali,* Vineet Tirth, Amnah Mohammed Alsuhaibani, Ali Algahtani, Tawfiq Al-Mughanam, Moamen S. Refat, Shafrida Sahrani,* and Muhammad Abrar

Cite This: *ACS Omega* 2023, 8, 29959−29965

Read Online

ACCESS | Metrics & More | Article Recommendations

ABSTRACT: Nanomaterials (NMs) with structural, optical, and dielectric properties are called functional or smart materials and have favorable applications in various fields of material science and nanotechnology. Pure and Co-doped $MgAl_2O_4$ were synthesized by using the sol−gel combustion method. A systematic investigation was carried out to understand the effects of the Co concentration on the crystalline phase, morphology, and optical and dielectric properties of Co-doped $MgAl_2O_4$. X-ray diffraction confirmed the cubic spinel structure with the $Fd\bar{3}m$ space group, and there was no impurity phase, while the surface morphology of the samples was investigated by scanning electron microscopy. The dielectric properties of the synthesized material are investigated using an LCR meter with respect to the variation in frequency (1−2 GHz), and their elemental composition has been examined through the energy-dispersive X-ray technique. The existence of the metal−oxygen Mg−Al−O bond has been confirmed by Fourier transform infrared spectroscopy. The value of the dielectric constant decreases with the increasing frequency and Co concentration. The optical behaviors of the Co^{2+}-doped $MgAl_2O_4$ reveal that the optical properties were enhanced by increasing the cobalt concentration, which ultimately led to a narrower band gap, which make them exquisite and suitable for energy storage applications, especially for super capacitors. This work aims to focus on the effect of cobalt ions in different concentrations on structural, optical, and dielectric properties.

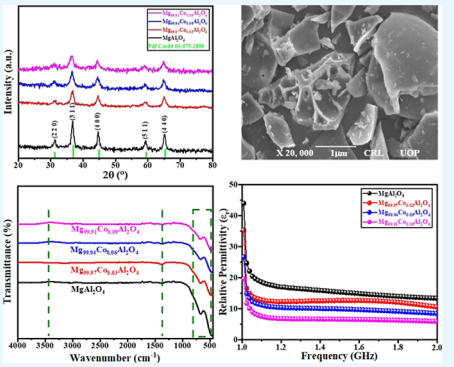

INTRODUCTION

Oxides having spinel-like structures are widely used in modern technology. Such functional materials are used for many purposes like humidity sensor, catalysts, optical windows, and so forth.[1−4] The spinel magnesium aluminate ($MgAl_2O_4$) is one of the most well-known structural materials having a large number of applications in various fields.[5,6] The spinel-like materials are used extensively in metallurgical, electrochemical, and chemical industries due to their outstanding optical and dielectric properties.[7−9] The spinel-type oxides have the general formula AB_2O_4, where A and B refer to two distinct cations of equal ionic sizes and are chemically and thermally stable.[10] The $MgAl_2O_4$ spinel crystal exhibits a cubic structure with space group ($Fd3m$).[11] The oxygen sublattice's spatial coordination has pseudo-cubical close packing. The cubic unit cell has 64 tetrahedral and 32 octahedral interstices between oxygen atoms. Al^{3+} inhabit 16 of the 32 octahedral interstices and Mg^{2+} fill 8 of the 64 tetrahedral interstices.[12]

The temperature affects the permittivity and ac conductivity of the nanoscale $MgAl_2O_4$ with frequency, and as a result, the real part of the dielectric constant and loss factor both increase with the temperature and decrease with frequency. Additionally, ac conductivity exhibits an opposite trend with frequency, although it continues to rise with a rise in temperature.[13,14] The valence electrons of the doped elements are impacted by transition metals of (3d) levels, which in turn affect the defect levels of the host material $MgAl_2O_4$. As a result of this interaction, the A- or B-site cations were insistently replaced with transition metal ions to attain the desired band structure tuning for certain applications. For instance, Fe^{2+} impurities dominate at the A-site of $MgAl_2O_4$ and subjugate their magnetic properties.[15] The optical behaviors' of the transition metal-doped $MgAl_2O_4$ depend on these two factors, valence and site type of the doped transition-metal ions.

Several researchers have investigated the dielectric behaviors of manganese-, chromium-, and iron-doped $MgAl_2O_4$ fabricated through the co-precipitation method and found that the modified value of relative permittivity was increased.[16] The continuous isomorphic between magnesium oxide and

Received: January 26, 2023
Accepted: May 24, 2023
Published: August 3, 2023

cobalt oxide is the foundation for the production of cobalt-doped $MgAl_2O_4$ samples; this allows for Co^{2+} ions to replace Mg^{2+} ions, which is attributed to their quite close ionic radii, and yields solid solutions of $Mg_{1-x}Co_xAl_2O_4$ ($0.00 \leq x \leq 0.09$).[17,18] Several researchers had adopted various techniques to fabricate the cobalt-doped $MgAl_2O_4$ such as sol−gel, microwave combustion, solid-state reactions, co-precipitation method, and so forth.[19] Only some researchers like Ullah et al. used the sol−gel combustion approach to prepare Co^{2+}-doped $MgAl_2O_4$.[4]

In this research work, an effort is made to synthesize the solid solution of $Mg_{1-x}Co_xAl_2O_4$ ($0.00 \leq x \leq 0.09$) spinel via a sol−gel combustion method. Due to the importance of this method, we studied the effect of Co^{2+} on the relationship between the structural, microstructural, vibrational, and dielectric properties (dielectric constant and tangent loss) of the $Mg_{1-x}Co_xAl_2O_4$ materials, which, by varying of the frequency, are improved.

RESULTS AND DISCUSSION

X-ray Diffraction Analysis. Figure 1 shows the X-ray diffraction (XRD) pattern of $Mg_{1-x}Co_xAl_2O_4$ ($0.00 \leq x \leq 0.09$) spinel solid solution. High intensity, sharp peaks with *hkl* values (220), (311), (400), (511), and (440) identified the samples' crystalline structure. The spinel cubic structure was confirmed by indexing of peaks, whose lattice constant is 8.08 Å, which matches exactly with PDF card # 01-075-1800 along with space group ($Fd\bar{3}m$). The spinel's single-phase cubic structure is confirmed by the absences of an impurity peak. For each composition, the XRD patterns have a high intensity peak at Braggs angle ($2\theta = 36°$), which correlate to the plane of (311).[20] It has been observed that the lattice constant of $MgAl_2O_4$ spinel increases with Co^{2+} contents. The variation in the lattice parameters is attributed to the slight difference in the ionic radii of cobalt ions (0.74 Å) and magnesium ions (0.65 Å). This increase in the lattice constant reveals that Mg^{2+} ions have been substituted by Co^{2+} ions in the crystal structure.[12,21] The volume of the unit cell increases with Co^{2+} contents and has been reported in this work. According to Vegard's law, the variations in the lattice parameters may be due to the ionic radius of the dopant element. However, most of cobalt−magnesium exchange occurs at the spinel's tetrahedral site.[22] Figure 1b shows the peaks shifting toward lower Bragg's angle because the ionic radius of the dopant material (Co^{2+}) is larger than that of the host material (Mg^{2+}).[23] The Sheerer equation is used to determine the average crystallite size of samples, as shown in eq 1.[24,25]

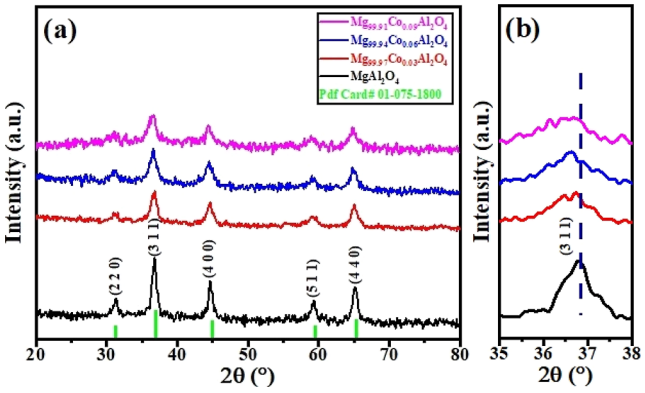

Figure 1. (a) XRD pattern of $Mg_{1-x}Co_xAl_2O_4$ ($0.00 \leq x \leq 0.09$) spinel calcined at 800 °C and (b) zoomed view of the (3 1 1) peak shifting toward the lower angle.

$$\text{Average crystallite size } (D) = \frac{K\lambda}{\beta_{hkl}\cos\theta} \quad (1)$$

The Williamson Hall analysis is used to calculate the lattice strain in the structure, as reported by Mote et al.[26] The dislocation density (δ) is determined by using this eq 2

$$\text{Dislocation density } (\delta) = \frac{1}{D^2} \quad (2)$$

The average crystallite size, dislocation density, lattice strain, and micro-strain of the synthesized samples are summarized in Table 1.

Table 1. Calculated Average Crystallite Size (D), Dislocation Density (δ), Lattice Strain (η), and Micro Strain (ε) of $Mg_{1-x}Co_xAl_2O_4$ ($0.00 \leq x \leq 0.09$) Spinel

parameters	$X = 0.00$	$X = 0.03$	$X = 0.06$	$X = 0.09$
average crystallite size "D" (nm)	34.241	39.125	51.570	54.135
dislocation density "δ" ($\times 10^{-3}$nm^{-2})	8.5300	6.7900	3.7600	3.6900
lattice strain "η" ($\times 10^{-2}$)	0.1013	0.0886	0.0672	0.0451
micro strain "ε" ($\times 10^{-2}$)	1.2367	1.0692	0.8531	0.7797

The XRD theoretical density (ρ_{th}) was determined from the relation

$$\rho_{th} = \frac{ZM}{N_A a^3} \quad (3)$$

where M is relative molecular mass, Z is that the number of atoms per unit cell, N_A is Avogadro's number, and a is the lattice parameter of $Mg_{1-x}Co_xAl_2O_4$ ($0.00 \leq x \leq 0.09$) spinel. Table 2 shows the physical properties like structural, lattice parameters, volume, density, and porosity of the solid solution of $Mg_{1-x}Co_xAl_2O_4$ ($0.00 \leq x \leq 0.09$) spinel. It has been observed that the porosity increases with the decreasing relative densities, as Co^{2+} was increased.[27] Porous materials are a class of materials with low density, large specific surface, and a range of novel properties in the electrical, mechanical, thermal, and acoustical fields.[28,29] The porosity was calculated by using eq 4.[30]

$$\text{Porosity} = \left(\frac{\rho_{th} - \rho_{exp}}{\rho_{th}}\right) \times 100\% \quad (4)$$

where ρ_{exp} is experimental and ρ_{th} is theoretical density.

Surface Morphological Studies. Figure 2a−d shows the scanning electron microscopy (SEM) micrograph of $Mg_{1-x}Co_xAl_2O_4$ ($0.00 \leq x \leq 0.09$) spinel calcined at 800 °C for 4 h in air. The size, shape, and grain boundary of all the samples are analyzed by using SEM. Figure 2a shows that the base sample exhibited a plate-like structure. The structure of the base sample is in accordance with the previous literature.[9,31] It was also found that the grain size decreases with the increasing Co^{2+} content. The lowest average grain size and maximum homogeneity were observed at $x = 0.06$. The morphology of the sample changes to that of nanotubes with Co^{2+} contents (at 3%), as shown in Figure 2b. Increasing the

https://doi.org/10.1021/acsomega.3c00541
ACS Omega 2023, 8, 29959−29965

Table 2. Variation of Physical Properties of $Mg_{1-x}Co_xAl_2O_4$ ($0.00 \leq x \leq 0.09$) Spinel with Co^{2+} Contents

contents (x)	structure	lattice parameters (nm)	volume (nm^3)	$\rho_{theoretical}$ (gm/cm^3)	$\rho_{experimental}$ (gm/cm^3)	$\rho_{relativedensity}$ (%)	porosity (%)
$X = 0.00$	cubic	0.808	0.528	3.58	3.56	99.6%	0.55%
$X = 0.03$	cubic	0.797	0.506	3.34	3.30	98.7%	1.19%
$X = 0.06$	cubic	0.793	0.499	3.10	3.01	97.2%	2.90%
$X = 0.09$	cubic	0.781	0.476	2.86	2.73	95.34	4.54%

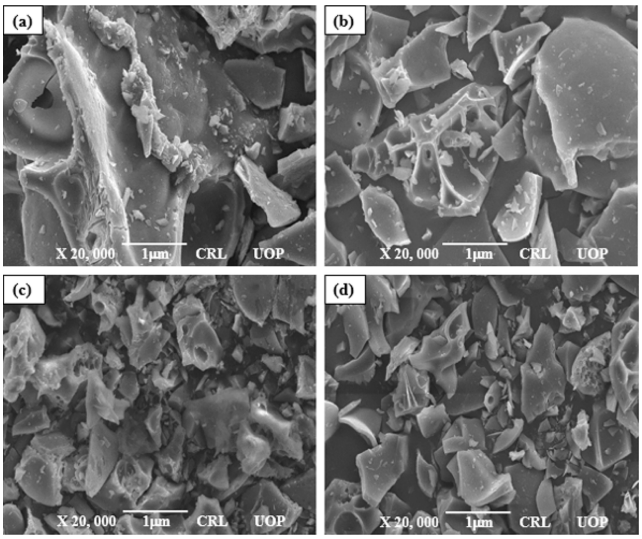

Figure 2. SEM micrograph of $Mg_{1-x}Co_xAl_2O_4$ ($0.00 \leq x \leq 0.09$) spinel (a) $x = 0.00$, (b) $x = 0.03$, (c) $x = 0.06$, and (d) $x = 0.09$.

cobalt content to 6% revealed the shifting morphology from nanotubes to the irregular shape, as shown in Figure 2c.

However, some large grains may be grown due to the agglomeration of the smaller grains.[24,32] The shape of the cobalt-doped magnesium aluminate changes into a disc with increasing Co^{2+} contents from 0.06 to 0.09, as shown in Figure 2d.[33]

The elemental composition of each sample is analyzed by using the energy-dispersive X-ray spectroscopy (EDX) technique. It confirms the presence of certain elements in the samples under investigation. Moreover, EDX analysis revealed the replacement of Mg^{2+} ions by Co^{2+} ions. Figure 3a–d shows the EDX pattern of $Mg_{1-x}Co_xAl_2O_4$ ($0.00 \leq x \leq 0.09$) spinel.

EDX patterns confirmed the presence of O, Mg, Al, and Co elements in the solid solution of $MgAl_2O_4$. The elemental composition of $Mg_{1-x}Co_xAl_2O_4$ ($0.00 \leq x \leq 0.09$) spinel is shown in Table 3.

Figure 4a–d shows the transmission electron microscopy (TEM) micrographs of $Mg_{1-x}Co_xAl_2O_4$ ($0.00 \leq x \leq 0.09$) spinel. The internal morphology and size of the synthesized pure and different cobalt-doped $MgAl_2O_4$ spinel are examined

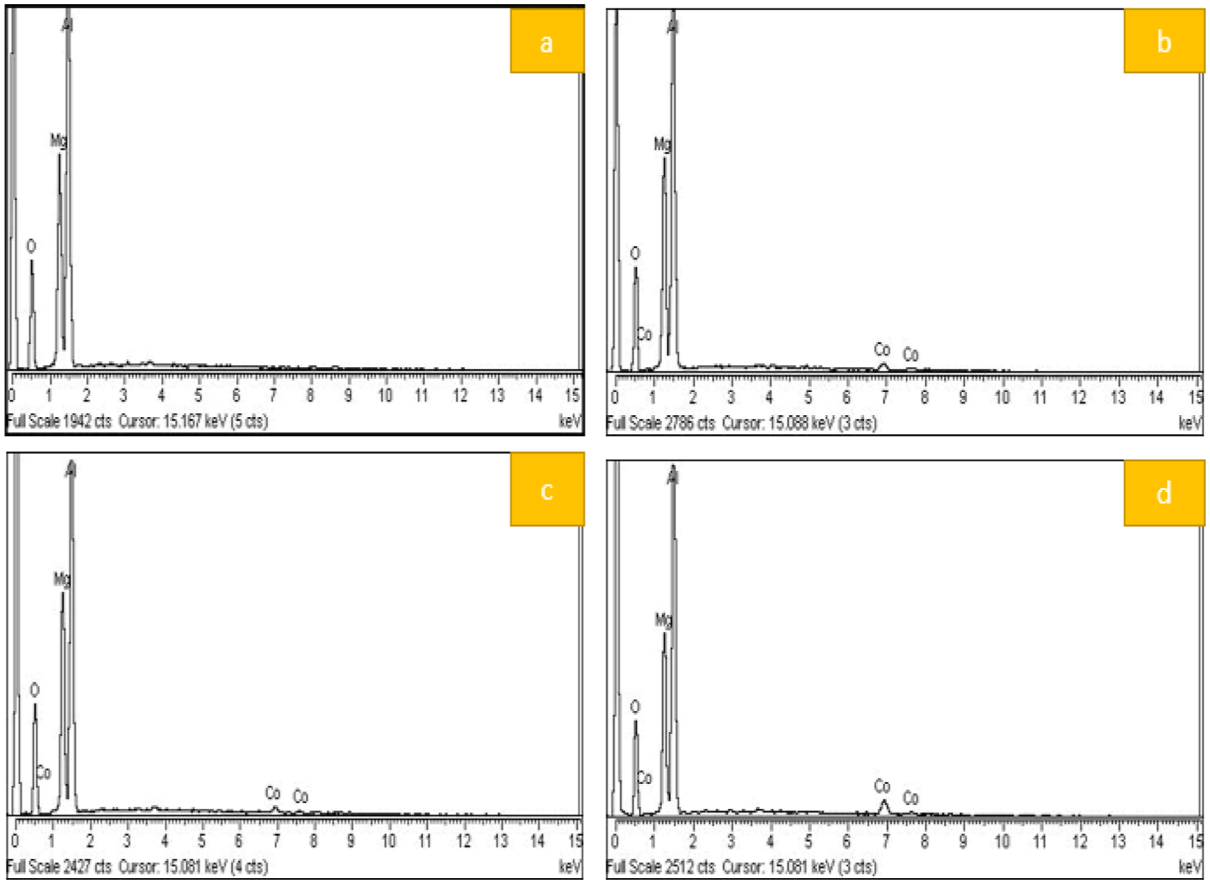

Figure 3. EDX spectra of $Mg_{1-x}Co_xAl_2O_4$ ($0.00 \leq x \leq 0.09$) spinel: (a) $x = 0.00$, (b) $x = 0.03$, (c) $x = 0.06$, and (d) $x = 0.09$.

https://doi.org/10.1021/acsomega.3c00541
ACS Omega 2023, 8, 29959−29965

Table 3. Elemental Composition of the Various Elements Present in the Synthesized Samples

elements	$X = 0.00$	$X = 0.03$	$X = 0.06$	$X = 0.09$
Mg	19.20	20.02	20.62	18.67
Al	44.80	41.70	40.91	42.08
O	36.00	34.41	35.45	31.80
Co		3.87	3.02	7.45
total (in %)	100	100	100	100

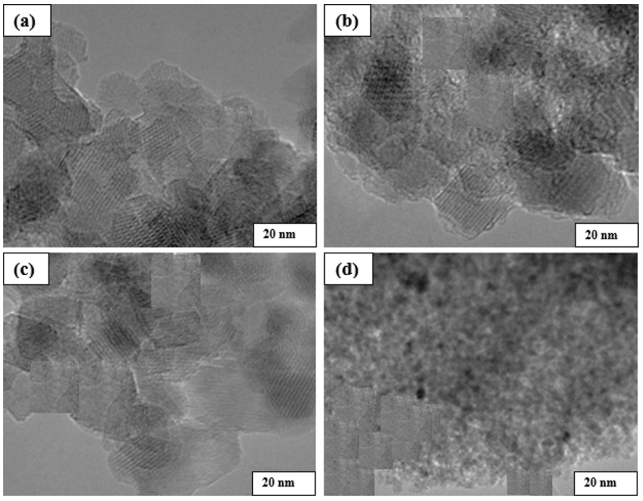

Figure 4. TEM micrographs of $Mg_{1-x}Co_xAl_2O_4$ ($0.00 \leq x \leq 0.09$) spinel: (a) $x = 0.00$, (b) $x = 0.03$, (c) $x = 0.06$, and (d) $x = 0.09$.

by using TEM. From the morphologies, it is clearly visible that highly crystalline, nanometer-sized ternary oxides were obtained. The doped Co displayed well-dispersed metal nanoparticles on the spinel support, as shown in Figure 4d.

OPTICAL PROPERTIES

UV−Visible Spectroscopy. The optical properties of $Mg_{1-x}Co_xAl_2O_4$ ($0.00 \leq x \leq 0.09$) spinel were examined by using UV−visible spectroscopy. The energy band gaps for all samples have been determined by using the TAUC, as shown in eq 5

$$(\alpha h\nu)^n = K(h\nu - E_g) \tag{5}$$

Figure 5a−d shows the UV spectra of $Mg_{1-x}Co_xAl_2O_4$ ($0.00 \leq x \leq 0.09$) spinel and reports that the band gap energy decreases from 4.09 to 2.79 eV with increasing Co^{2+} contents. This is due to the minor difference of ionic radii of Co^{2+} (0.67 Å) and Mg^{2+} (0.65 Å).[34]

The high band gap values of $MgAl_2O_4$ may be attributed to the s−p hybridization between the 3s and 3p of Mg and Al, respectively, which causes the lowest energy levels in the conduction band to be filled.[35] On the basis of two distinct cation symmetries, Mg^{2+} (A) and Al^{+3} (B) are used to reveal the optical behavior of 3d transition metals (Co, Ni, and Mn)-doped $MgAl_2O_4$ (AB_2O_4) spinel. The Co^{2+} ($3d^7$) ions at the A-site with T_d symmetry exhibit a high band gap energy due to their high excitation energy (over 3.30 eV).[36]

FTIR Study. The Fourier transform infrared (FTIR) spectroscopic analysis revealed information about bonding and phase composition of the samples recorded in the range of wave number 400−4000 cm^{-1}, as shown in Figure 6.

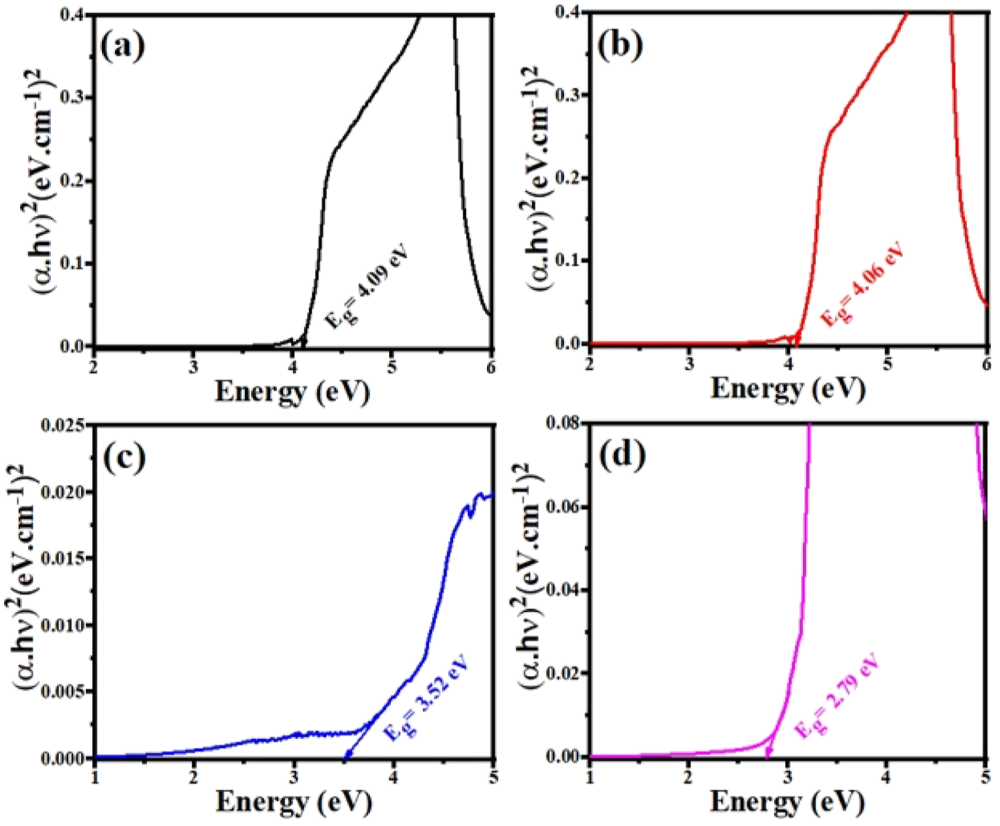

Figure 5. UV spectra of $Mg_{1-x}Co_xAl_2O_4$ ($0.00 \leq x \leq 0.09$) spinel: (a) $x = 0.00$, (b) $x = 0.03$, (c) $x = 0.06$, and (d) $x = 0.09$.

https://doi.org/10.1021/acsomega.3c00541
ACS Omega 2023, 8, 29959−29965

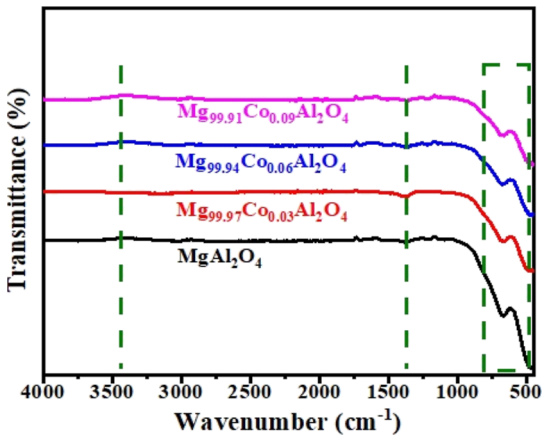

Figure 6. FTIR spectrum of $Mg_{1-x}Co_xAl_2O_4$ ($0.00 \leq x \leq 0.09$) spinel.

The frequency range 500−900 cm^{-1} shows the stretching vibrational mode of aluminum−oxygen (Al−O), metal−oxygen (M−O), and metal−oxygen−aluminum (M−O−Al) for the spinel structure.[37] The existence of the nitrate group is confirmed by the absorption at about 1380 cm^{-1}.[38] Also, the absorption band in the 1200−1600 cm^{-1} of the absorption spectra reveals that the Mg^{2+} is substituted by Co^{2+} ions and occupy the tetrahedral sites of the spinel $MgAl_2O_4$ nanocrystallites in all spectra. The band about 3480 cm^{-1} is attributed to the (O−H) vibrations of the water molecules, which are absorbed by the samples.[39]

Microwave Dielectric Properties. In the current research work, the dielectric properties, that is, relative permittivity and tangent loss, have been measured by using impedance spectroscopy at the frequency range (from 1 to 2 GHz). The dopant concentration affected the dielectric permittivity and loss of the $Mg_{1-x}Co_xAl_2O_4$ ($0.00 \leq x \leq 0.09$) spinel.[40] The value of relative permittivity of the base sample decreases with the increasing Co^{2+} contents, as shown in Figure 7.

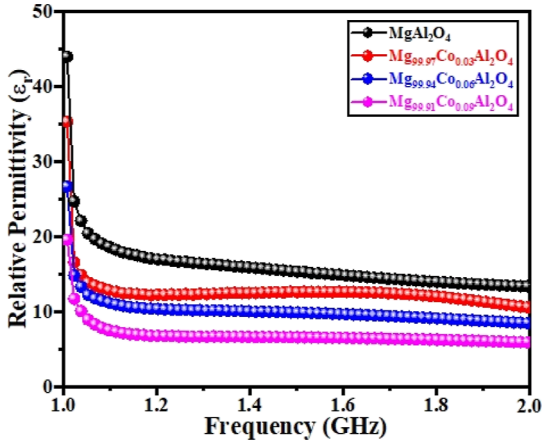

Figure 7. Variation of the dielectric constant with Co concentration and frequency of $Mg_{1-x}Co_xAl_2O_4$ ($0.00 \leq x \leq 0.09$) spinel.

The obtained values of relative permittivity for pure and doped samples are 44, 35, 27, and 20 at 1 GHz frequency. Figure 6 also shows that the value of relative permittivity decreases with the increasing operating frequency. The value of relative permittivity could be explained easily according to the relative dipole moments and lattice structure of the sample.[41] In the structure of $MgAl_2O_4$ spinel, the permanent dipole moment attained the Centro symmetric position on *c*-axis, which modifies the value of relative permittivity. It is concluded that the smaller the c/a ratio, the lower will be the value of relative permittivity.[42] A Co-doped $MgAl_2O_4$ compound is suitable for the application of the humidity sensor, data storage devices, and communication technology.[14,18,29] Figure 8 shows the plot of tangent loss (tan δ) versus operating frequency for the pure and doped $MgAl_2O_4$ sample.

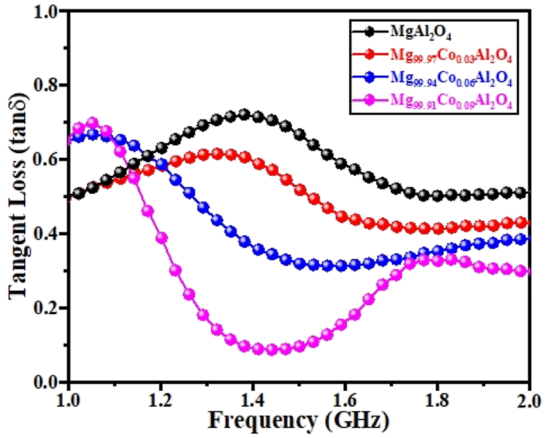

Figure 8. Variation of dissipation factor of $Mg_{1-x}Co_xAl_2O_4$ ($0.00 \leq x \leq 0.09$) spinel with frequency.

Figure 8 shows that the tangent loss decreases with the increasing operating frequency and Co^{2+} contents, which may be due to the accumulation of charge carriers and thermal activation energy.[43] The tangent loss values show fluctuations with frequency, which may be due to the substitution of a lower ionic cation (Mg^{2+}) by a higher ionic cation (Co^{2+}). The frequency-dependent tangent loss is a dimensionless quantity, and it is good for base station applications.[44]

CONCLUSIONS

The solid solution of $Mg_{1-x}Co_xAl_2O_4$ ($0.00 \leq x \leq 0.09$) spinel has been synthesized by the sol−gel combustion method. The XRD studies reveal that Co^{2+}-doped $MgAl_2O_4$ exhibits a cubic structure. The base and doped samples have same lattice parameters. The spinel structure was unchanged by the substitution of the Co^{2+} cation. The SEM micrograph shows that the surface morphologies change with Co^{2+} contents from a plate-like shape to irregular nanotubes. The EDX studies confirm the existence of Al, Mg, O, and Co elements. The FTIR analysis suggested the existence of the M-Al-O bond. The improved optical properties have been reported by doping of Co^{2+} concentrations. The band gap energy and dielectric constant decrease with the increasing doping concentrations without the structure distortion. The overall findings may help in the application of smart technology.

Materials and Experimental Procedure. The solid solution of $Mg_{1-x}Co_xAl_2O_4$ ($0.00 \leq x \leq 0.09$) is synthesized by using the sol−gel combustion method. The chemical precursors used to synthesize the samples are aluminum nitrate ($Al(NO_3)_3 \cdot 9H_2O$), magnesium nitrate ($Mg(NO_3)_2 \cdot 6H_2O$), cobalt nitrate ($Co(NO_3)_2 \cdot 6H_2O$), and citric acid ($C_6H_8O_7 \cdot H_2O$), and they are mixed with an appropriate stoichiometric ratio. All the precursor chemicals were purchased from Sigma-Aldrich with a minimal purity research rating of 99.96%. The

https://doi.org/10.1021/acsomega.3c00541
ACS Omega 2023, 8, 29959−29965

solution of all the raw materials is blended in a beaker at a 1:2 molar ratio. The anhydrous citric acid was used as a combustible fuel catalyst. The citric acid and metal nitrates are both taken in an equal stoichiometric ratio. In order to obtain a homogeneous and thick gel of solution, all the chemicals are poured into a beaker that contained 25 mL of deionized water and then heated continuously and stirred for an hour at 120 °C on a hot plate. The whole procedure is carried out in a ventilated enclosure. The specimens were then inserted in a muffle furnace at 400 °C for combustion by a fierce exothermic reaction. To achieve the desired phase of spinel aluminates, the fine powder of each composition was calcined at 800 °C for 4 h. The Co^{2+} ions are substituted on the A-site of AB_2O_4 i−e Mg-site cation.

Characterizations. The absolute information of the cell volume, crystallite size, structural lattice strain, lattice constants, and the crystal structure was obtained by crystallographic studies using Panalytical X'Pert software. The grain size was determined using ImageJ software. The microstructural and phase analysis was performed using SEM (JSM-5910, JEOL Japan) and XRD (JDX-3532, JEOL, Japan) with Cu Kα radiation (λ = 0.154 nm). The elemental composition of each sample was analyzed by (EDX) spectroscopy using the Oxford Inca X-Act to verify the existence of the probable elemental contents. The absorption spectra of the (FTIR) were obtained on a Perkin-Elmer GX FTIR system with a resolution of 10 cm^{-1} in the 400−4000 cm^{-1} range to study the bond and functional group attached to the samples. The optical properties were studied by using ultraviolet−visible spectroscopy. The absorption spectra of the samples were investigated using a Perkin-Elmer UV−vis Spectrometer, λ = 25, in the visible range. An LCR meter was employed to measure the dielectric properties of the sintered sample (1−2 GHz)..

AUTHOR INFORMATION

Corresponding Authors

Abid Zaman − *Department of Physics, Riphah International University, Islamabad 44000, Pakistan;* orcid.org/0000-0001-9527-479X; Email: zaman.abid87@gmail.com

Asad Ali − *Department of Physics, Riphah International University, Islamabad 44000, Pakistan; Department of Physics, Government Post Graduate College, Nowshera 24100 Khyber Pakhtunkhwa, Pakistan*; Email: kasadiiui@gmail.com

Shafrida Sahrani − *Institute of Visual Informatics, Universiti Kebangsaan Malaysia, Bangi 43600, Malaysia*; Email: shafrida@ukm.edu.my

Authors

Kamran Ullah − *Department of Physics, Hazara University, Mansehra 21300, Pakistan;* orcid.org/0000-0003-0047-3812

Shoaib Ali Khan − *Department of Physics, Hazara University, Mansehra 21300, Pakistan*

Mahidur R. Sarker − *Institute of Visual Informatics, Universiti Kebangsaan Malaysia, Bangi 43600, Malaysia*

Vineet Tirth − *Mechanical Engineering Department, College of Engineering, King Khalid University, Abha 61421 Asir, Kingdom of Saudi Arabia; Research Center for Advanced Materials Science (RCAMS), King Khalid University, Abha 61413 Asir, Kingdom of Saudi Arabia;* orcid.org/0000-0002-8208-7183

Amnah Mohammed Alsuhaibani − *Department of Physical Sport Science, College of Education, Princess Nourah bint Abdulrahman University, Riyadh 11671, Saudi Arabia*

Ali Algahtani − *Mechanical Engineering Department, College of Engineering, King Khalid University, Abha 61421 Asir, Kingdom of Saudi Arabia; Research Center for Advanced Materials Science (RCAMS), King Khalid University, Abha 61413 Asir, Kingdom of Saudi Arabia*

Tawfiq Al-Mughanam − *Department of Mechanical Engineering, College of Engineering, King Faisal University, Al-Ahsa 31982, Saudi Arabia*

Moamen S. Refat − *Department of Chemistry, College of Science, Taif University, Taif 21944, Saudi Arabia*

Muhammad Abrar − *Department of Physics, Hazara University, Mansehra 21300, Pakistan*

Complete contact information is available at: https://pubs.acs.org/10.1021/acsomega.3c00541

Notes

The authors declare no competing financial interest.

ACKNOWLEDGMENTS

This research was funded by Universiti Kebangsaan Malaysia under Grant Code GGPM-2021-050 and GGPM-2022-064. The authors extend their appreciation to the Deanship of Scientific Research at King Khalid University Abha 61421, Asir, Kingdom of Saudi Arabia for funding this work through the Large Groups Project under grant number RGP.2/142/44. Princess Nourah bint Abdulrahman University Researchers Supporting Project number (PNURSP2023R65), Princess Nourah bint Abdulrahman University, Riyadh, Saudi Arabia.

REFERENCES

(1) Mary Jacintha, A.; Manikandan, A.; Chinnaraj, K.; Arul Antony, S.; Neeraja, P. Comparative studies of spinel $MnFe_2O_4$ nanostructures: structural, morphological, optical, magnetic and catalytic properties. *J. Nanosci. Nanotechnol.* **2015**, *15*, 9732−9740.

(2) Suguna, S.; Shankar, S.; Jaganathan, S. K.; Manikandan, A. Novel synthesis and characterization studies of spinel $Ni_xCo_{1-x}Al_2O_4$ (x= 0.0 to 1.0) nano-catalysts for the catalytic oxidation of benzyl alcohol. *J. Nanosci. Nanotechnol.* **2018**, *18*, 1019−1026.

(3) Zeb, M.; Tahir, M.; Muhammad, F.; Gul, Z.; Wahab, F.; Sarker, M. R.; Alamgeer; Ali, S.; Ilyas, S. Z. Pyrrol-Anthracene: Synthesis, Characterization and Its Application as Active Material in Humidity, Temperature and Light Sensors. *Coatings* **2022**, *12*, 848.

(4) Ullah, F.; Qureshi, M. T.; Abbas, S. K.; Atiq, S.; Ikhlaq, U.; Iqbal, Z.; Anwar, M. S.; Saleem, M.; Anwar, M. S. Dilute magnetic ions mediated magneto-dielectric, optical and ferroelectric response of $MgAl_2O_4$ spinels. *J. Phys.: Condens. Matter* **2020**, *32*, 365701.

(5) Tavangarian, F.; Emadi, R. Synthesis and characterization of pure Nano crystalline magnesium aluminate spinel powder. *J. Alloys Compd.* **2010**, *489*, 600−604.

(6) Singh, V.; Chakradhar, R. P. S.; Rao, J. L.; Kim, D. K. Synthesis, characterization, photoluminescence and EPR investigations of Mn doped $MgAl_2O_4$ phosphors. *J. Solid State Chem.* **2007**, *180*, 2067−2074.

(7) Salmones, J.; Galicia, J. A.; Wang, J. A.; Valenzuela, M. A.; Aguilar-Rios, G. Synthesis and characterization of nanocrystallite $MgAl_2O_4$ spinels as catalysts support. *J. Mater. Sci. Lett.* **2000**, *19*, 1033−1037.

(8) Tahir, M.; Ilyas, M.; Aziz, F.; R Sarker, M.; Zeb, M.; Ibrahim, M. A.; Mohamed, R. Fabrication and microelectronic properties of hybrid organic−inorganic (poly (9, 9, dioctylfluorene)/p-Si) heterojunction for electronic applications. *Appl. Sci.* **2020**, *10*, 7974.

(9) Tsai, M. T.; Chang, Y. S.; Huang, I. B.; Pan, B. Y. Luminescent and structural properties of manganese-doped zinc aluminate spinel Nano crystals. *Ceram. Int.* **2013**, *39*, 3691−3697.
(10) Duan, X.; Pan, M.; Yu, F.; Yuan, D. Synthesis, structure and optical properties of $CoAl_2O_4$ spinel Nano crystals. *J. Alloys Compd.* **2011**, *509*, 1079−1083.
(11) Sickafus, K. E.; Wills, J. M.; Grimes, N. W. Structure of spinel. *J. Am. Ceram. Soc.* **2004**, *82*, 3279−3292.
(12) Belyaev, A.; Basyrova, L.; Sysoev, V.; Lelet, M.; Balabanov, S.; Kalganov, V.; Mikhailovski, V.; Baranov, M.; Stepanidenko, E.; Vitkin, V.; et al. Microstructure, doping and optical properties of Co2+:ZnAl2O4 transparent ceramics for saturable absorbers: Effect of the ZnF2 sintering additive. *J. Alloys Compd.* **2020**, *829*, 154514.
(13) Kurien, S.; Sebastian, S.; Mathew, J.; George, K. Structural and electrical properties of nano-sized magnesium aluminate. *Indian J. Pure Appl. Phys.* **2004**, *42*, 926−933.
(14) Tahir, M.; Zeb, M.; Hussain, S.; Hussain, S.; Sarker, M. R.; Khan, D. N.; Wahab, F.; Ali, S. H. M. Cuprous oxide nanoparticles: Synthesis, characterization, and their application for enhancing the humidity-sensing properties of poly (dioctylfluorene). *Polymers* **2022**, *14*, 1503.
(15) Ahmad, J.; Koch-Müller, M. Effect of substitution of K^+ ions on the structural and electrical properties of nanocrystalline $MgAl_2O_4$ spinel oxide. *Phys. Rev. B: Condens. Matter Mater. Phys.* **2011**, *406*, 3484.
(16) Iqbal, M. J.; Ismail, B. Electric, dielectric and magnetic characteristics of Cr^{3+}, Mn^{3+} and Fe^{3+} substituted $MgAl_2O_4$: effect of pH and annealing temperature. *J. Alloys Compd.* **2009**, *472*, 434−440.
(17) Amini, M. M.; Mirzaee, M.; Sepanj, N. The effect of solution chemistry on the preparation of $MgAl_2O_4$ by hydrothermal-assisted sol−gel processing. *Mater. Res. Bull.* **2007**, *42*, 563−570.
(18) Nordin, N. A.; Mohamed, M. A.; Salehmin, M. N. I.; Mohd Yusoff, S. F. Photocatalytic active metal−organic framework and its derivatives for solar-driven environmental remediation and renewable energy. *Coord. Chem. Rev.* **2022**, *468*, 214639.
(19) Akhtar, M. N.; Javed, S.; Ahmad, M.; Sulong, A. B.; Khan, M. A. Sol gel derived MnTi doped Co2 W-type hexagonal ferrites: structural, physical, spectral and magnetic evaluations. *Ceram. Int.* **2020**, *46*, 7842−7849.
(20) Khattab, R. M.; Sadek, H. E. H.; Gaber, A. A. Synthesis of $Co_xMg_{1-x}Al_2O_4$ nanospinel pigments by microwave combustion method. *Ceram. Int.* **2017**, *43*, 234−243.
(21) Alagu Raja, E.; Menon, S.; Dhabekar, B.; Rawat, N. S.; Gundu Rao, T. Investigation of defect centres responsible for TL/OSL in $MgAl_2O_4$: Tb^{3+}. *J. Lumin.* **2009**, *129*, 829−835.
(22) Ghaedamini, A.; Sobhani, M. Effect of Cobalt Doping on Synthesis and Sintering Properties of $MgAl_2O_4$ Spinel Nano powders. *J. Mater. Eng. Perform.* **2021**, *30*, 390−395.
(23) Choudhary, A. K.; Dwivedi, A.; Bahadur, A.; Yadav, T. P.; Rai, S. B. Enhanced up conversion emission and temperature sensor sensitivity in presence of Bi3+ ions in Er^{3+}/Yb^{3+} co-doped $MgAl_2O_4$ phosphor. *Ceram. Int.* **2018**, *44*, 9633−9642.
(24) Ahmed, K.; Mehboob, N.; Zaman, A.; Ali, A.; Mushtaq, M.; Ahmad, D.; Ahmed, N.; Sultana, F.; Bashir, K.; Amami, M.; et al. Enhanced the Cu2+ doping on the structural, optical and electrical properties of zinc oxide (ZnO) nanoparticles for electronic device applications. *J. Lumin.* **2022**, *250*, 119112.
(25) Syed, A.; Sohail Khan, A.; Ullah, A.; Sarker, M. R.; Tahir Khan, M.; Ali, A.; Tirth, V.; Zaman, A.; Ur Rashid, H.; Zaman, A. Enhancement of the phase, optical and dielectric studies of Bi0. 5Na0. 5TiO3 (BNT) based structure ceramics. *J. Saudi Chem. Soc.* **2023**, *27*, 101617.
(26) Mote, V. D.; Purushotham, Y.; Dole, B. N. Williamson-Hall analysis in estimation of lattice strain in nanometer-sized ZnO particles. *J. Theor. Appl. Phys.* **2012**, *6*, 6−8.
(27) Belyaev, A.; Basyrova, L.; Sysoev, V.; Lelet, M.; Balabanov, S.; Kalganov, V.; Mikhailovski, V.; Baranov, M.; Stepanidenko, E.; Vitkin, V.; et al. Microstructure, doping and optical properties of Co2+:ZnAl2O4 transparent ceramics for saturable absorbers: Effect of the ZnF2 sintering additive. *J. Alloys Compd.* **2020**, *829*, 154514.
(28) Yasrebi, N.; Moghaddas, J. Study on the Effect of Humidity on Electrical Properties of Copper-Silica Aerogel. *Iran. J. Chem. Eng.* **2015**, *12*, 3−12.
(29) Petrila, I.; Tudorache, F. Annealing Temperature Effects on Humidity Sensor Properties for Mg0. 5W0. 5Fe2O4 Spinel Ferrite. *Sensors* **2022**, *22*, 9182.
(30) Ali, A.; Uddin, S.; Lal, M.; Zaman, A.; Iqbal, Z.; Althubeiti, K. Structural, optical and microwave dielectric properties of Ba (Ti1−xSnx) 4O9, 0≤ x≤ 0.7 ceramics. *Sci. Rep.* **2021**, *11*, 17889.
(31) Shang-Pan, H.; Zhi-Qiang, W.; Xiao-Juan, W.; Ji-Wen, S. Optical properties of Cr doped ZnAl2O4 nanoparticles with Spinel structure synthesized by hydrothermal method. *Mater. Res. Express* **2020**, *7*, 015025.
(32) WS, R. *ImageJ*; US National Institutes of Health: Bethesda, Maryland, USA, 2014; pp 1997−2012.
(33) Tian, Y.; Guo, Y.; Jiang, M.; Sheng, Y.; Hari, B.; Zhang, G.; Zhou, B.; Zhu, Y.; Wang, Z.; Jiang, Y.; Wang, Z. Synthesis of hydrophobic zinc borate nanodiscs for lubrication. *Mater. Lett.* **2006**, *60*, 2511−2515.
(34) Kanwal, K.; Ismail, B.; Rajani, K. S.; Kissinger, N. J.; Zeb, A. Effect of Co2+ ions doping on the structural and optical properties of magnesium aluminate. *J. Electron. Mater.* **2017**, *46*, 4206−4213.
(35) El-Fadl, A. A.; Abd-Elrahman, M. I.; Younis, N.; Afify, N.; Abu-Sehly, A. A.; Hafiz, M. M. Syntheses of new spinels $Zn_{1-x}Fe_xAl_2O_4$ nanocrystallines structure: Optical and magnetic characteristics. *J. Alloys Compd.* **2019**, *795*, 114−119.
(36) Izumi, K.; Miyazaki, S.; Yoshida, S.; Mizokawa, T.; Hanamura, E. Optical properties of 3d transition-metal-doped $MgAl_2O_4$ spinels. *Phys. Rev. B: Condens. Matter Mater. Phys.* **2007**, *76*, 075111.
(37) Dhak, D.; Pramanik, P. Particle size comparison of soft-chemically prepared transition metal (Co, Ni, Cu, Zn) aluminate spinels. *J. Am. Ceram. Soc.* **2006**, *89*, 1014−1021.
(38) Duan, X.; Yuan, D.; Luan, C.; Sun, Z.; Xu, D.; Lv, M. Microstructural evolution of transparent glass-ceramics containing Co^{2+}: $MgAl_2O_4$ nanocrystals. *J. Non-Cryst. Solids* **2003**, *328*, 245−249.
(39) Luan, C.; Yuan, D.; Duan, X.; Sun, H.; Zhang, G.; Guo, S.; Pan, D.; Shi, X.; Li, Z.; Sun, Z.; Li, Z. Synthesis and characterization of Co^{2+}: $MgAl_2O_4$ nanocrystal. *J. Sol-Gel Sci. Technol.* **2006**, *38*, 245−249.
(40) Ullah, A.; Khan, A. S.; Sarker, M. R.; Iqbal, M. J.; Khan, H. U.; Tirth, V.; Zaman, A.; Algahtani, A.; Zaman, A. Investigation of Dielectric, Ferroelectric, and Strain Responses of (1-x)[0.90 (Bi 0.5 Na 0.5) TiO 3-0.10 SrTiO 3]-xCuO Ceramics. *ACS Omega* **2023**, *8*, 12372−12378.
(41) Zaman, A.; Uddin, S.; Mehboob, N.; Ali, A. Structural investigation and improvement of microwave dielectric properties in Ca (HfxTi1-x) O3 ceramics. *Phys. Scr.* **2020**, *96*, 025701.
(42) Qin, W.; Muche, D. N. F.; Castro, R. H. R.; van Benthem, K. The effect of electric fields on grain growth in MgAl2O4 spinel. *J. Eur. Ceram. Soc.* **2018**, *38*, 5512−5518.
(43) Păcurariu, C.; Lazău, I.; Ecsedi, Z.; Lazău, R.; Barvinschi, P.; Mărginean, G. New synthesis methods of MgAl2O4 spinel. *J. Eur. Ceram. Soc.* **2007**, *27*, 707−710.
(44) Ganesh, I.; Johnson, R.; Rao, G. V. N.; Mahajan, Y. R.; Madavendra, S. S.; Reddy, B. M. Microwave-assisted combustion synthesis of nanocrystalline MgAl2O4 spinel powder. *Ceram. Int.* **2005**, *31*, 67−74.

https://doi.org/10.1021/acsomega.3c00541
ACS Omega 2023, 8, 29959−29965